

Evidence for a Bright-Edged Jet in the Optical/NIR Afterglow of GRB 160625B

ROBERT STRAUSBAUGH,¹ NATHANIEL BUTLER,² WILLIAM H. LEE,³ ELEONORA TROJA,^{4,5} AND ALAN M. WATSON³¹*Department of Physics, Arizona State University*²*School of Earth and Space Exploration, Arizona State University*³*Instituto de Astronomía, Universidad Nacional Autónoma de México*⁴*Department of Astronomy, University of Maryland*⁵*NASA Goddard Space Flight Center*

(Accepted ApJ)

ABSTRACT

Using deep and high-cadence gamma-ray burst (GRB) afterglow data from RATIR, we observe a sharp and achromatic light curve break 12.6 days after the GRB, accompanied by an approximately achromatic bump. Fitting of the optical, NIR, and X-ray data suggest a very narrow (2 degree) jet which remains collimated at late-time. We argue that the sharp light curve bump suggests an edge brightened jet, perhaps emitting only during a brief period of lateral jet expansion. The lightcurve also exhibits a gradual spectral evolution lasting > 10 days. The evolution of the flux can be modeled as $\text{Flux} \sim \left(\frac{t}{[20\text{days}]}\right)^\alpha \left(\frac{\lambda}{[800\text{nm}]}\right)^\beta$, with a temporal slope $\alpha = -0.956 \pm 0.003$ and a gradually time-varying spectral slope $\beta = (0.60 \pm 0.07) + (0.26 \pm 0.06)\log\left(\frac{t}{[20\text{days}]}\right)$.

1. INTRODUCTION

GRB 160625B was detected by NASA’s Fermi Gamma-ray Space Telescope’s γ -ray burst monitor (Meegan, et al. 2009) as a one-second long pulse (Dirirsa, et al. 2016). Automatic follow up by the Large Area Telescope (Atwood, et al. 2009) resulted in detection of another bright, but longer lasting (≈ 30 seconds) pulse about three minutes later. This later pulse peaked at a visual magnitude of 7.9, and a secondary peak exhibiting significant polarization was detected 16 seconds later by the MASTER-IAC telescope (Lipunov, et al. 2010). We focus here on late-time, afterglow data in the *riZYZH* bands captured with the Reionization And Transients Infra-Red/Optical camera (RATIR) (Butler, et al. 2012) which features spectral evolution and a sharp bump in the light curve that were not modeled in (Troja, et al. 2017). Over fifty observing nights after the GRB, we are able to measure a so-called “jet break” with unprecedented cadence and sensitivity across multiple optical/NIR bands. We also study *Swift* X-ray and Ultra-Violet (UV) data captured during the same epoch.

These data potentially allow us to obtain unique constraints on the jetting of the afterglow and the possibility of lateral expansion of the jet. At early times, the high bulk Lorentz factor, $\Gamma \approx 10^3$, of the outflow permit us to view only a narrow region of angular size $1/\Gamma$ of the jet. The polarization detected by MASTER peaked at $8 \pm 0.5\%$ (Troja, et al. 2017), suggestive of a jet viewing angle which is slightly off-axis. As the blast wave decelerates, more of the jet becomes visible. Once $1/\Gamma \sim \theta_{\text{jet}}$, the edge of the jet becomes visible and the flux begins declining more rapidly as the energy per solid angle begins decreasing (Rhoads 1997, 1999; Rybicki & Lightman 1979). The edges of the jet come into causal contact at about this point, and the jet can potentially begin spreading laterally (see, e.g., Wygoda, Waxman, & Frail 2011; van Eerten & MacFadyen 2012; Granot & Piran 2012). If the jet spreads, it can effectively halt the blast wave expansion and further decrease the afterglow flux (Rhoads 1999; Sari, Piran, & Halpern 1999; Granot, et al. 2001; Wygoda, Waxman, & Frail 2011).

Detailed observations and accurate models for jet breaks are critical because they allow us to determine opening angle of the jet (Frail, et al. 2001), which is crucial in turn for understanding GRB energetics (Freedman & Waxman 2001; Wygoda, et al. 2016; Sari, Piran, & Halpern 1999; Kocevski & Butler 2008; Ghirlanda, Ghisellini, & Lazzati

2004; Ghirlanda, et al. 2013; Amati, et al. 2002) and rates (Rhoads 1997; Wanderman & Piran 2010; Butler, Bloom, & Poznanski 2010; Jimenez & Piran 2013; Fenimore, E. E., & Ramirez-Ruiz 2000). In addition, high-cadence observations with small error bars (as we have here) can potentially allow us to measure the energy and velocity structure of the jet (e.g., Granot & Kumar 2003; Rossi, et al. 2002; Kumar & Granot 2003; Postnov, Prokhorov, & Lipunov 1999) and to constrain the hydrodynamical processes that potentially lead to a spreading jet (Sari, Piran, & Halpern 1999; Granot, et al. 2001; Mao & Wang 2001; Zhang, et al. 2006).

2. ANALYSIS

RATIR photometry for GRB 160625B in the *riZYZH* bands, reduced as described in Troja, et al. (2017), along with measurements reported by the *Swift* UVOT and XRT are shown in Figure 1. A dominant feature in the RATIR and XRT data is an apparently achromatic temporal “jet-break” at a time of about 12 days. Interestingly, there is a slight brightening (i.e. the temporal power-law decay is less steep around the jet break than at early times) present just prior to this jet-break. The feature is present in all the RATIR bands with comparable amplitude, suggesting a color similar to that of the afterglow. The jet-break, and the brief re-brightening just before it, can be seen more clearly in the inset of Figure 1, where the RATIR data have been normalized with respect to the early *H*-band behavior.

Table 1. Light Curve Fitting Parameters

Band	θ_1	θ_{jet}	$B(\%)$	α_1	α_2	χ^2/ν
<i>r</i>	1.75 ± 0.05	2.40 ± 0.05	22.0 ± 2.1	0.971 ± 0.002	1.59 ± 0.06	1.31
<i>i</i>	1.90 ± 0.10	2.40 ± 0.05	18.6 ± 1.9	0.966 ± 0.002	1.64 ± 0.05	1.10
<i>Z</i>	2.00 ± 0.15	2.35 ± 0.05	23.4 ± 3.6	0.953 ± 0.004	1.58 ± 0.10	0.87
<i>Y</i>	1.95 ± 0.25	2.35 ± 0.05	17.8 ± 4.6	0.931 ± 0.005	1.73 ± 0.21	0.80
<i>J</i>	1.95 ± 0.35	2.35 ± 0.15	29.8 ± 9.8	0.904 ± 0.005	1.37 ± 0.16	2.91
<i>H</i>	1.15 ± 0.50	2.80 ± 1.10	23.3 ± 12.5	0.880 ± 0.006	2.19 ± 0.90	1.65
<i>UV</i>	1.013 ± 0.032	...	0.32
<i>X-ray</i>	...	2.5 ± 0.3	< 20.5 (1- σ)	1.202 ± 0.022	2.06 ± 0.22	1.64

Fitting parameters from the solid line models plotted in Figures 1 and 3, corresponding to Equation 2.

The Swift XRT data (Figure 1), reduced using our automated pipeline¹, show a power-law decline in flux as $t^{-1.20 \pm 0.02}$ prior to the break. The spectrum, with a mean count rate of 0.014 cps (0.3-10 keV), is well-fitted ($\chi^2/\nu = 68.57/75$) by an absorbed power-law with photon index $\Gamma = 2.07 \pm 0.06$ and an absorbing column of $N_H = 4.4 \pm 0.1 \times 10^{21} \text{ cm}^{-2}$ at $z = 1.406$ in addition to the Galactic absorbing column. The mean unabsorbed flux is $(103 \pm 5) \text{ nJ}$ at 1 keV.

Assuming the standard external shock model (e.g., Sari, Piran, & Narayan 1998) for a constant density circum-burst medium (CBM), in the slow-cooling regime with a cooling break below the X-ray band, the X-ray temporal and spectral indices imply and are consistent with a power-law index for the shocked electrons of $p = 2.26 \pm 0.03$. Assuming the optical/NIR bands are below the cooling break, the implied temporal decay is $t^{-0.94 \pm 0.02}$. This is similar to the typical decay laws we observe (Figure 1; Table 1), although the observed indices are not constant across the optical/NIR bands. The early-time optical/NIR spectral energy distribution (SED) is consistent with the expected $F_\nu \propto \nu^{-0.6}$ ($F_\lambda \propto \lambda^{0.24}$ in Figure 2) spectrum, absorbed by $A_V \sim 0.1$ of SMC-type dust (Pei 1992). The 1 keV to *r*-band flux ratio (~ 50 ; Figure 1) is consistent with a cooling break initially near the X-ray band.

The temporal decay law in the optical/NIR bands flattens slightly with increasing wavelength (Figure 1, inset; Table 1). The data are well-fitted as $\alpha(\lambda) = (0.938 \pm 0.003) - 2.5(0.08 \pm 0.01)\log(\lambda/[980\text{nm}])$. The result is a slow and continuous reddening that yields an optical/NIR SED (Figure 2) described by a gradually steepening power-law index, $\beta = (0.60 \pm 0.07) + (0.26 \pm 0.06)\log(\frac{t}{20\text{days}})$, reaching $F_\lambda \propto \lambda^{0.6-0.7}$ by the end of the observation. The evolution of the spectral power law index – likely due to a gradual passage of the synchrotron spectrum beginning prior to our observations – may or may not continue through the jet-break (Figure 2, inset). The color transition prior to 10 days is gradual and smooth, with no break in either the spectrum or lightcurve. We see no evidence for any strong spectral

¹ <http://butler.lab.asu.edu/swift>

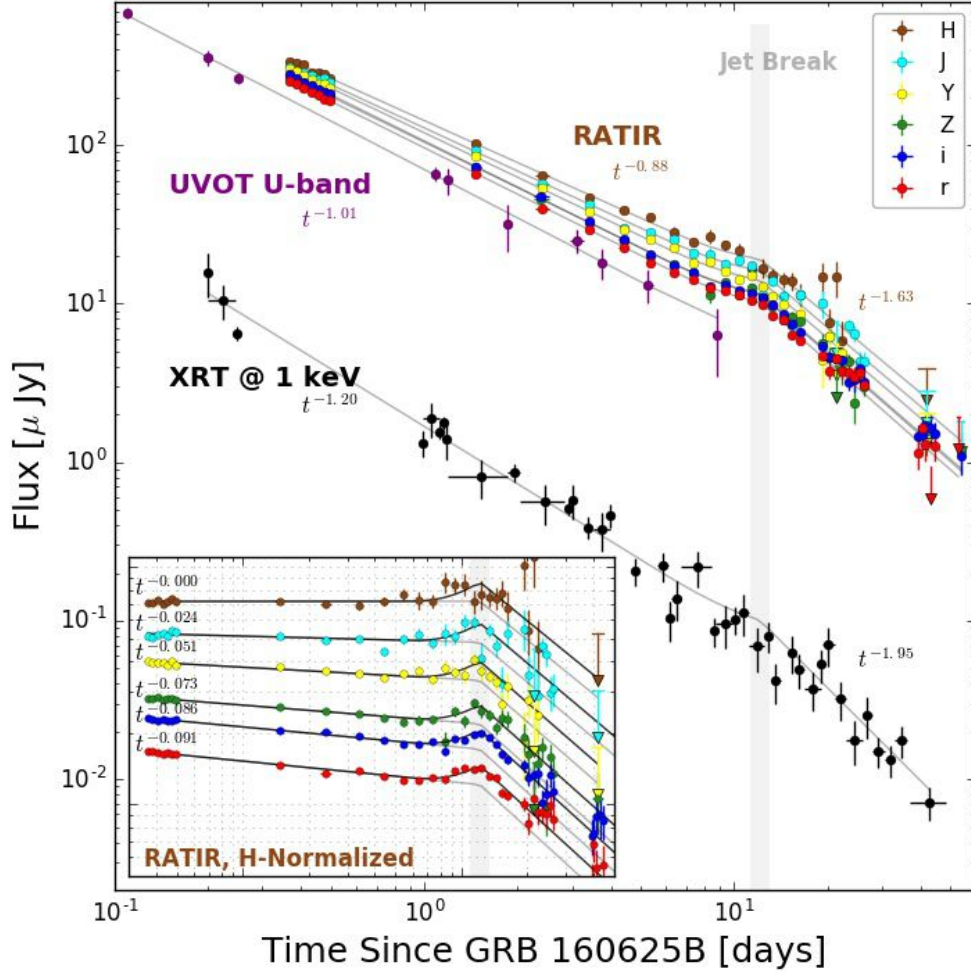


Figure 1. The afterglow lightcurve for GRB 160625B in the *riZYZJH* bands from RATIR. X-ray and UV data are from *Swift*. The inset lightcurves are normalized by the early time *H*-band to better display the jet break and bump. The data in both graphs are fit with the model described in Section 2. Additional information about the fits can be found in Table 1. The data presented in this figure can be found in the Appendix.

evolution during the jet break, with the synchrotron cooling frequency likely to be above the RATIR bandpass until at least approximately 30 days after the GRB.

We determine the jet opening angle, $\theta_{\text{jet}} = \Gamma(t_{\text{jet}})^{-1}$, using the jet break time t_{jet} as

$$\theta_{\text{jet}} = \Gamma^{-1}(t_{\text{jet}}) = 3.27 \left(\frac{t_{\text{jet}}}{\text{days}} \right)^{3/8} \left(\frac{1+z}{2} \right)^{-3/8} \left(\frac{E_{\text{iso}}}{10^{53} \text{ erg}} \right)^{-1/8} \left(\frac{\eta}{0.2} \right)^{1/8} \left(\frac{n}{0.1 \text{ cm}^{-3}} \right)^{1/8} = 2.28 \left(\frac{t_{\text{jet}}}{12.6 \text{ days}} \right)^{3/8} \text{ degrees} \quad (1)$$

(Frail, et al. 2001). Here, we have inserted values for the redshift z , the isotropic energy in γ -rays E_{iso} , the efficiency of converting the ejecta kinetic energy into γ -rays η , and the CBM density n from Troja, et al. (2017). If we make the simplifying assumption that we are viewing the jet exactly on-axis, we can use Equation 1 to convert between observed time and the observable extent of the jet $1/\Gamma(t)$. The light curve can then be divided by the empirical, wavelength-dependent, early-time decay law to reconstruct the apparent jet profile $F_j(\theta = 1/\Gamma)$ (Figure 3).

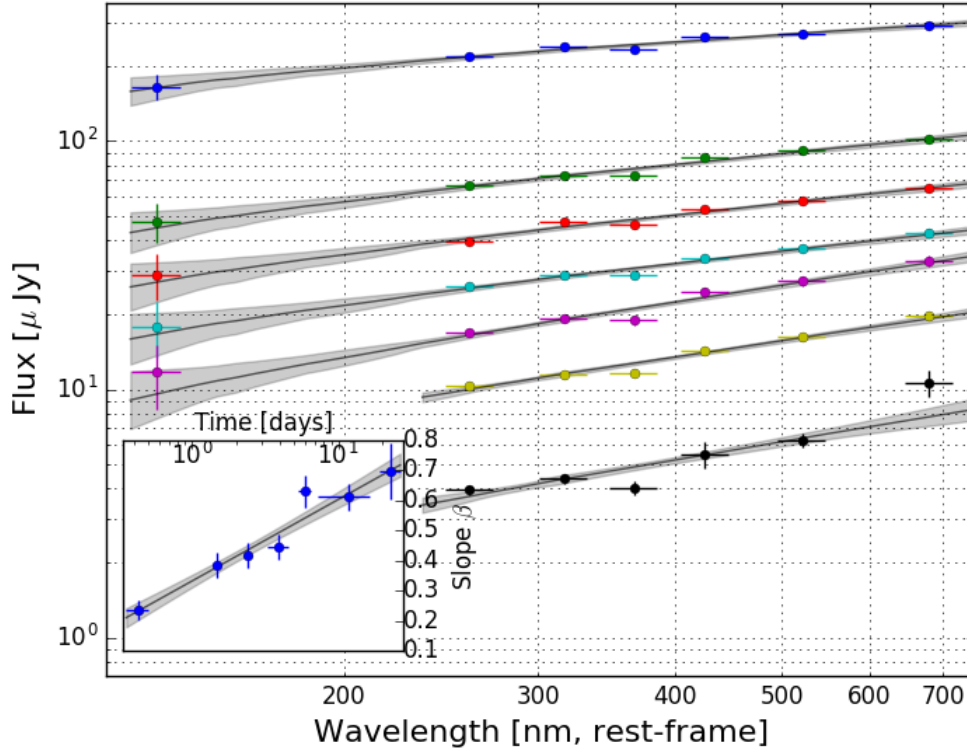


Figure 2. The spectral evolution of GRB 160625B over the RATIR bands, as well as UV from *Swift*. The data are fit with a power law attenuated by SMC extinction (Pei 1992). The inset shows the evolution of the spectral power-law index, β , over time; the power-law index and fit statistics can be found in Table 2. The data presented in this figure can be found in the Appendix.

Table 2. SED Fitting Parameters

Time (days)	β	χ^2/ν
0.36-0.51	0.24 ± 0.07	0.96
1.41-1.52	0.39 ± 0.07	1.40
2.27-2.52	0.42 ± 0.07	1.61
3.30-4.53	0.45 ± 0.07	1.36
5.31-6.45	0.63 ± 0.08	2.50
7.30-16.41	0.61 ± 0.07	3.42
19.25-26.51	0.70 ± 0.11	5.84

Fits for the power-law models describing the spectral evolution of GRB 160625B plotted in Figure 2; all models are fit using an $A_V = 0.05 \pm 0.04$ in SMC law extinction (Pei 1992) in the host galaxy.

We discuss the relation between $F_j(\theta)$ and the jet emissivity $j(\theta)$ in detail below in Section 3. In the uniform, or homogeneous, jet model (e.g. Rhoads 1997; Sari, Piran, & Halpern 1999), $F_j = 1$ until the edge of the jet becomes visible at $1/\Gamma = \theta_{\text{jet}}$. After this time, in the absence of jet spreading, $F_j(\theta) = (\theta_{\text{jet}}\Gamma)^2$, and the flux steepens by a factor $(t/t_{\text{jet}})^{-3/4}$ in time. This model fits the data well at early and late time in all bands (see, Figure 1). However, the lightcurve bump that occurs near the jet break requires an additional component. We assume a phenomenological

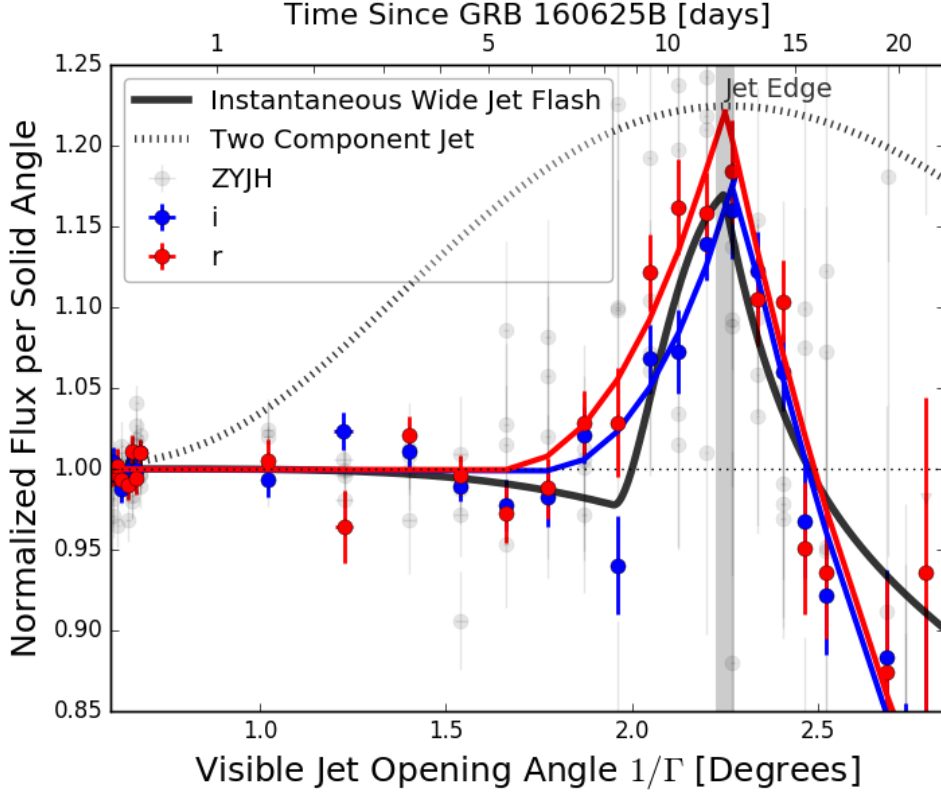


Figure 3. The emissivity of GRB 160625B’s jet with respect to jet angle for all bands (with i and r bands highlighted), showing a structured jet with bright edges. The blue and red curves are the model shown in Equation 2; the black and gray curves show physical models derived in Section 3 for two-component jets.

model:

$$F_j(\theta = 1/\Gamma) = \begin{cases} 1, & \theta \leq \theta_1 \\ 1 + B(\theta - \theta_1)^2/(\theta_{\text{jet}} - \theta_1)^2, & \theta_1 < \theta \leq \theta_{\text{jet}} \\ 1 + B(\theta_{\text{jet}}/\theta)^2, & \theta > \theta_{\text{jet}} \end{cases} \quad (2)$$

The apparent jet flux $F_j(\theta)$ is constant until $1/\Gamma = \theta_1$, after which point it increases quadratically by a limb-brightening factor B at the edge of the jet, θ_{jet} . We find that all bands are well-fitted by such a model with consistent values for the parameters (Table 1). The X-ray data do not require a bump, but they also cannot rule out the optical/NIR bump at $> 1\sigma$ significance ($\Delta\chi^2 = 2.28$ for 2 additional degrees of freedom). The model is also overplotted in Figure 1 using the mean fit parameters ($\theta_1 = 1.80 \pm 0.05^\circ$, $\theta_{\text{jet}} = 2.40 \pm 0.03^\circ$, $B = 20.5 \pm 1.2\%$) to compute $t^{-\alpha(\lambda)} F_j(\theta)$.

3. DISCUSSION

Bumps of varying shapes and sizes have been observed in GRB afterglows. A contemporaneous supernova (SN) can cause a re-brightening in the afterglow lightcurves (Bloom, et al. 1999; Hjorth & Bloom 2012). However, at $z = 1.406$ (Xu, et al. 2016; D’Elia, Melandri, & Malesani 2016), typical SNe (absolute magnitude $M = -19$) would be 5 magnitudes fainter than the bump in Figure 1. The bump has a red color consistent with that of the afterglow, quite unlike the very blue color of the brightest SNe (e.g., Dong, et al. 2016). Furthermore, SNe have very broad temporal brightening features (e.g., Bloom, et al. 1999), very different from the sharp bump in the afterglow of GRB 160625B. Reprocessing the afterglow light by dust in the CBM can, in principle, generate bumps in the NIR but not typically in the r band (e.g., Waxman & Draine 2000; Esin & Blanford 2000). As the optical transition from reverse-shock to forward-shock dominated emission is early ($t < 1$ day; Troja, et al. 2017), it is not likely to contribute the sharp bump 10 days after GRB 160625b.

X-ray flaring is a common effect seen in many early afterglows (e.g., Galama, et al. 1998), although no early flaring is detected in the afterglow of GRB 160625B. Attributed to a central engine that is still active (Li, et al. 2012; Galama, et al. 1998), these features are similarly narrow in time – $dt/t \sim 0.1$ for early (e.g., Chincarini, et al. 2007) and late (e.g., Curran, et al. 2008) flares – but refreshed shocks typically occur within hours of the GRB (Panaiteescu, Meszaros, & Rees 1998; Li, et al. 2012) and also exhibit harder spectra than the afterglow (e.g., Butler & Kocinski 2007). It is important to note that there is no observed change to the color evolution in the SED around the time of the re-brightening.

It seems most natural to assume that the increase in flux just before the jet break is not coincidental, but that the phenomena are related. However, it is important to note that the effects of relativistic beaming would permit a jet with bright edges (e.g., as implied in Equation 2 above, or Kumar & Granot 2003) to be observed at quite early time, yielding smooth temporal variations in the observed flux with $dt/t \sim 1$. A jet with a bright edge that does not change with time would produce a wide bump in the light curve starting at earlier times than the bump in Figure 3. To see this, we can derive the observed jet structure starting with a model for the rest-frame emissivity j' of the jet. The expected flux is

$$f_\nu(t) = 2\pi D\Gamma^{-2} \int \varphi^2 d\varphi \int \frac{j'_\nu(t', \Omega') d\mu}{(1 - \beta\mu)^2 (1 - \mu^2)^{3/2}} \quad (3)$$

(see, Woods & Loeb 1999), where D is the distance from the source to the observer and φ is the angle to the jet edge as viewed by the observer. Here, $\beta = v/c$ and $\Gamma = 1/\sqrt{1 - \beta^2}$; μ is the cosine of the angle between the velocity and the direction of the observer. We now assume a spherical blast wave traveling directly toward the observer and an infinitesimally thin emitting shell with zero emissivity beyond an angle $\theta = \theta_{\text{jet}}$:

$$j' = A_0 t'^{-a} \nu'^{-b} \delta(r - \beta ct) H(\theta_{\text{jet}} - \theta). \quad (4)$$

Here, a is the power-law temporal index and b is the power-law spectral index. The rest-frame time, t' , and the lab-frame time, t , are related by $t' = t + r\mu/c$, and r is the radius of the blast wave. The function H is the Heaviside function. Following Woods & Loeb (1999), we can use the delta function to integrate over the viewing angle φ to obtain:

$$f_\nu(t) = 2\pi\beta A_0 \left(\frac{c}{D}\right)^2 \frac{t^{2-a} \nu^{-b} (1 - \beta)^{4-a+b}}{\Gamma^{2+b} (4 - a + b)} \left(1 - \left[\frac{(1 - \beta)}{(1 - \beta\mu_{\text{min}})}\right]^{4-a+b}\right), \quad (5)$$

with $\mu_{\text{min}} = \cos(\theta_{\text{jet}})$. The term in the square brackets goes to zero at early time, and the pre-factor is the flux due to a spherical, non-jetted blast wave, $f_{\nu, \text{sphere}}$. Defining, $F_j = f_\nu / f_{\nu, \text{sphere}}$, we have:

$$F_j = 1 - [(1 - \beta)/(1 - \beta\mu_{\text{min}})]^{4-a+b} \approx 1 - (1 + (\Gamma\theta_{\text{jet}})^2)^{-n}, \quad (6)$$

where we have taken the small angle limit. Like F_j above in Equation 2, this function is constant ($F_j = 1$) at early time and then falls like $(\Gamma\theta_{\text{jet}})^2 \sim t^{-3/4}$ at late time, due to the relationship, $\Gamma \propto t^{-3/8}$, seen in Equation 1. The index $n \approx 4$ affects the sharpness of the break, since the flux decays as $t^{-\alpha} \nu^{-b}$, $\alpha = 1/4 + a/4 + 3b/8$ and $n = 5 - 4\alpha + 5b/2$. The indices α and b above and below the cooling break are constrained by closure relations and, in terms of the electron power law index p , $n = 11/2 - p/2$ and $n = 7(1 - p/4)$ below and above the cooling break, respectively. Hence, for $p = 2$, we expect a slightly sharper break below the cooling break ($n = 4.5$) than above the cooling break ($n = 3.5$).

A narrow jet (θ_1) with a large Γ enveloped by a wider jet (θ_2) with a smaller Γ can be modeled from Equation 6 as $F_j(\theta_1) + (1 + B)(F_j(\theta_2) - F_j(\theta_1))$. Plotted in Figure 3 (as Two Component Jet), this model shows that relativistic beaming does not simply restrict the observer to view a portion $1/\Gamma$ of the jet. Rather, because the emissivity versus angle is convolved with the relative Doppler factor, $1 + (\Gamma\theta)^2$, to some power, a jet with an increased edge emissivity tends to produce temporally broad light curve variations ($dt/t \approx 1$). Some mechanism must be invoked to introduce additional time dependence. A natural mechanism is the lateral spreading of the jet, which can begin around the jet break time because the entire surface of the jet is just coming into causal contact at that point. Granot (2007) argue that the jet angle should increase as $\theta_{\text{jet}} \approx \theta_1 + c_s/(c\Gamma)$, where c_s is the sound speed, leading to an approximately constant relative Doppler factor during the expansion. The function F then remains flat for longer. More recent work on jet expansion points towards a slower logarithmic jet expansion (van Eerten & MacFadyen 2012; Zhang & MacFadyen 2009) as opposed to a fast exponential expansion (Sari, Piran, & Halpern 1999; Granot, et al. 2001; Mao & Wang 2001).

To produce a narrow bump, we invoke the possibility of an instantaneous flash of emission, modeled by replacing H in Equation 4 by $H + j'_e(\theta)\delta(t' - t'_1)t'_1$. Here, $j'_e(\theta)$ is a dimensionless, relative emissivity which is zero within θ_1 . For $\theta > \theta_1$, we define $j'_e(\theta) = B(\theta - \theta_1)^2/(\theta_{\text{jet}} - \theta_1)^2$ (cf. Equation 2). With this addition, F_j (Equation 6) becomes:

$$F_j = 1 - [1 + (\Gamma\theta_{\text{jet}})^2]^{-n} + n\left(\frac{t}{t_1}\right)^{-n} j_e\left(\theta = \frac{1}{\Gamma}\sqrt{\frac{t - t_1}{t_1}}\right), \quad (7)$$

where t_1 is the observer-frame time corresponding to θ_1 . This model is plotted in Figure 3, with $B = 26.4\%$.

Jets with either homogeneous or a brighter central region (Granot & Kumar 2003), viewed on-axis, are not expected to have an increase in their afterglow light curves. Jets with a brighter central region viewed slightly off-axis, may be able to cause a brief re-brightening before the jet break. If viewed from an angle not directly along the central axis of the jet, but still inside the jet opening angle ($0 < \theta_{\text{view}} < \theta_{\text{jet}}$), the observer could detect an increase in flux as the brighter center of the jet came into view. However, with these viewing conditions, we expect to see more complicated jet-break behavior on long time-scales ($dt/t \sim 1$; see, e.g., Kumar & Granot 2003). Jet models are considered in Kumar & Granot (2003) which have a Gaussian energy profile and more exotic jet structures – such as ring- or fan-shaped jets (Granot 2007) – exhibit more complex afterglow behavior (e.g. multiple jet breaks). Two-component jets (Peng, Konigl, & Granot 2005; Racusin et al. 2008) create smoother bumps at earlier times (e.g. the two-component jet plotted in Figure 3), that are not consistent with our short-duration bump and the ensuing rapid steepening by $(\Gamma\theta_{\text{jet}})^2 \sim t^{-3/4}$.

It is also important to note that the functional form of this steepening is inconsistent with the hypothesis of continued lateral expansion of the jet. That expansion tends to halt the radial expansion of the fireball, producing a rapid flux decline in all bands proportional to t^{-p} (see, Sari, Piran, & Halpern 1999). We rule out that scenario at the $> 4\sigma$ level (Table 1), apparently consistent with hydrodynamical simulations (e.g., Kumar & Granot 2003). Although we think lateral expansion does not persist at late time for this afterglow, we do think it is important near the jet break time. It is a brief period of lateral expansion lasting $dt/t \approx df/f \approx 0.2$ that allows material just outside the primary jet ($\theta > \theta_1$ in Equation 2) to be shocked and to emit radiation. Interestingly, the spectral evolution we observe for this event (Section 2) represents a gradual loss of total blast wave energy of about 10% as compared to canonical models involving spectral/temporal breaks (e.g., Sari, Piran, & Narayan 1998). It could be that this energy reservoir, lurking near the edge of the jet, is tapped to make the bump during a brief period of lateral jet expansion.

4. CONCLUSION

With regular, nightly *riZYYH* band observations over a period of weeks – yielding a $\lesssim 3\%$ typical photometric precision lightcurve – we are able to probe the internal jet structure of the afterglow to GRB 160625B in unprecedented detail. We observe a brief re-brightening in the afterglow light curve during the jet-break (Figure 1). We model this increase in flux by invoking a structured jet with bright edges (Figure 3), emitting instantaneously as the jet expands laterally for a brief period. This interpretation is driven largely by the simultaneity of the bump and break. The primary alternative bump explanation surviving the arguments above – a weak pulse due to continued central engine activity – cannot be ruled-out by the X-ray data, which do not show a clear bump but are consistent with one. An admittedly more-pronounced X-ray bump does coincide with a probable jet break in the case of the flaring GRB 050502B (e.g., Falcone, et al. 2006; Curran, et al. 2008). Moreover, there is at least one case (e.g., Berger, et al. 2000) of a similar multi-band optical bump present just before and not precisely simultaneous with a well-studied jet break.

We also observe a wavelength-dependent temporal evolution in the afterglow to GRB 160625B prior to the jet break, with temporal index $\alpha = 0.938 - 0.2 \log(\lambda/[980 \text{ nm}])$. Following the break, the temporal decay indices are consistent with those expected for a sharp-edged jet (increase by $3/4$), with no lateral expansion.

GRB 160625B exhibits a very sharply defined jet break corresponding to a very narrow jet opening angle, $\theta_{\text{jet}} \approx 2^\circ$, indicative of nearly-on-axis viewing of a highly relativistic outflow impinging on a low density external medium (see, also, Troja, et al. 2017). Typical jets should be observed at an angle $\theta_{\text{view}} = \frac{2}{3}\theta_{\text{jet}}$ and may or may not exhibit pronounced lateral expansion. Both effects can introduce variations with $dt \approx t$ (e.g., Granot 2007) and can tend to make jet break signatures in light curves less distinct. Whatever mechanism created the bump for GRB 160625B (Figure 1) also contributed to making a more distinct jet break, and this effect may or may not be common. Additional deep, high-cadence, late-time observations are required to uncover the light curve diversity and to yield a better understanding of why jet breaks are so challenging to detect and measure in the *Swift*-era (e.g., Panaitescu 2007).

5. ACKNOWLEDGEMENTS

We thank the RATIR project team and the staff of the Observatorio Astronómico Nacional on Sierra San Pedro Mártir, and acknowledge the contribution of Leonid Georgiev and Neil Gehrels to its development. RATIR is a collaboration between the University of California, the Universidad Nacional Autónoma de México, NASA Goddard Space Flight Center, and Arizona State University, benefiting from the loan of an H2RG detector and hardware and software support from Teledyne Scientific and Imaging. RATIR, the automation of the Harold L. Johnson Telescope of the Observatorio Astronómico Nacional on Sierra San Pedro Mártir, and the operation of both are funded through NASA grants NNX09AH71G, NNX09AT02G, NNX10AI27G, and NNX12AE66G, CONACyT grants INFR-2009-01-122785 and CB-2008-101958, UNAM PAPIIT grant IN113810, and UC MEXUS-CONACyT grant CN 09-283.

REFERENCES

- Amati, L., Frontera, F., Tavani M., et al. 2002, *A&A*, 390, 81
- Atwood, W. B., Abdo, A. A., Ackermann, M., et al. 2009, *ApJ*, 697, 1071-1102
- Berger, E., Sari, R., Frail, D. A., et al. 2000, *ApJ*, 545, 56
- Bloom, J. S., Kulkarni, S. R., Djorgovski, et al. 1999, *Nature*, 401, 453456
- Butler N.R., Bloom J.S., & Poznanski D., 2010, *ApJ*, 711, 495
- Butler, N., Klein, C., Fox, O., et al. 2012, *Proc SPIE*, 8446, 844610
- Butler, N. R., & Kocevski, D. 2007, *ApJ*, 663, 407
- Chincarini, G., Moretti, A., Romano, P., et al. 2007, *ApJ*, 671, 1903-1920
- Curran, P., Starling, R., O'Brien, P., et al. 2008, *A&A*, 487, 533-538
- D'Elia, V., Melandri, A., & Malesani, A. 2016 *GCN* 19601
- Dirirsa, F., Racusin J., McEnery J., & Desiante R. 2016 *GCN* 19580
- Dong, S., Shappee, B. J., Prieto, J. L., et al. 2016, *Science*, 351, 257
- Esin, A. A., & Blandford, R. 2000, *ApJL*, 534, L151
- Falcone, A. D., Burrows, D. N., Lazzati, D., et al. 2006, *ApJ*, 641, 1010
- Fenimore, E. E., & Ramirez-Ruiz, E. 2000, *arXiv:astro-ph/0004176*
- Frail, D. A., Kulkarni, S. R., Sari, R., et al. 2001, *ApJ*, 562, L55
- Freedman, D. L., & Waxman, E. 2001, *ApJ*, 547, 922
- Galama, T. J., Groot, P. J., van Paradijs, J., et al. 1998, *ApJ*, 497, L13-L16
- Ghirlanda, G., Ghisellini, G., & Lazzati D. 2004, *ApJ*, 616, 331
- Ghirlanda, G., Ghisellini, G., Salvaterra, R. et al., 2013, *MNRAS*, 428, 14101423
- Granot, J., Miller, M., Piran, T., Suen, W. M., & Hughes, P. A. 2001, in *GRBs in the Afterglow Era*, ed. E. Costa, F. Frontera, & J. Hjorth (Berlin: Springer), 312
- Granot, J. & Kumar, P. 2003, *ApJ*, 591, 1086-1096
- Granot, J. 2007, *RMxAA*, 27, 140
- Granot, J., & Piran, T. 2012, *MNRAS*, 421, 570
- Hjorth, J., & Bloom, J. S., 2012, Chapter 9 in “Gamma-Ray Bursts, Cambridge Astrophysics Series 51, eds. C. Kouveliotou, R. A. M. J. Wijers and S. Woosley, Cambridge University Press (Cambridge), p. 169-190, 169
- Jimenez, R., & Piran, T. 2013, *ApJ*, 773, 126
- Kocevski, D., & Butler, N. 2008, *ApJ*, 680, 531
- Kumar, P., & Granot, J. 2003, *ApJ*, 591, 1075-1085
- Li, L., Liang, E., Tang, Q., et al. 2012, *ApJ*, 758, 1
- Lipunov, V., Kornilov, V., Gorbovskoy, E., et al. 2010, *AdASt*, 2010, 349171
- Mao, J., & Wang, J., 2001, *Chin. J. Astron. Astrophys.*, 1, 349
- Meegan, C., Lichti, G., Bhat, P. N., et al. 2009, *ApJ*, 702, 1
- Panaitescu, A., Meszaros, P., & Rees, M. J. 1998, *ApJ*, 503, 314
- Panaitescu, A. 2007, *MNRAS*, 380, 374-380
- Pei, Y. C. 1992, *ApJ*, 395, 130
- Peng, F., Konigl, A., Granot, J., 2005, *ApJ*, 626, 966
- Postnov, K. A., Prokhorov, M. E., & Lipunov V. M. 2001, *ARep*, 45, 236-240.
- Racusin, J. L., Karpov, S. V., Sokolowski, M., et al. 2008, *Nature*, 455, 7210, 183-188
- Rhoads, J. E. 1997, *ApJL*, 487, L1
- Rhoads, J. E. 1999, *ApJ*, 525, 2
- Rossi, E., Lazzati, D., Salmonson, J. D., & Ghisellini, G. 2002, *astro-ph/0211020*
- Rybicki, G. B. & Lightman, A. P. 1979, *Radiative Processes in Astrophysics* (New York: Wiley)
- Sari, R., Piran, T., & Narayan, R. 1998, *ApJL*, 497, L17
- Sari, R., Piran, T., & Halpern, J. P. 1999, *ApJL*, 519, L17
- Troja, E., Lipunov, V. M., Mundell, C. G., et al. 2017a, *Nature*, 547, 425-427
- van Eerten, H. J., & MacFadyen, A. I. 2012, *ApJ*, 751, 155
- Wanderman D., Piran T., 2010, *MNRAS*, 406, 1944
- Waxman, E., & Draine, B. T. 2000, *ApJ*, 537, 796

- Woods, E., & Loeb, A. 1999, ApJ, 523, 187
- Wygoda, N., Waxman, E., & Frail, D. A. 2011, ApJ, 738, L23
- Wygoda, N., Guetta, D., Mandich, M. A., & Waxman, E., ApJ, 824, 127
- Xu, D., Malensani, D., Fynbo, J. P. U., et al. 2016, GCN 19600
- Zhang B., Fan Y. Z., Dyks J., et al 2006, ApJ, 642, 354
- Zhang, W. & MacFadyen A. 2009, ApJ, 698, 1261-1272

APPENDIX

Table 3. RATIR GRB 160625B Data

Days after GRB	Exposure (minutes)	r	i	Z	Y	J	H
0.37	1.2	18.24 \pm 0.01	18.05 \pm 0.01	17.99 \pm 0.01	17.90 \pm 0.01	17.79 \pm 0.01	17.65 \pm 0.02
0.39	1.2	18.29 \pm 0.01	18.11 \pm 0.01	18.03 \pm 0.01	17.96 \pm 0.01	17.85 \pm 0.01	17.69 \pm 0.02
0.41	1.2	18.35 \pm 0.01	18.17 \pm 0.01	18.08 \pm 0.01	18.01 \pm 0.01	17.87 \pm 0.01	17.71 \pm 0.02
0.43	1.2	18.43 \pm 0.01	18.23 \pm 0.01	18.16 \pm 0.01	18.07 \pm 0.02	17.92 \pm 0.01	17.82 \pm 0.01
0.45	1.2	18.46 \pm 0.01	18.28 \pm 0.01	18.20 \pm 0.01	18.14 \pm 0.02	17.99 \pm 0.01	17.83 \pm 0.01
0.48	1.2	18.52 \pm 0.01	18.33 \pm 0.01	18.23 \pm 0.01	18.15 \pm 0.01	17.97 \pm 0.01	17.85 \pm 0.01
0.50	1.2	18.55 \pm 0.01	18.36 \pm 0.01	18.30 \pm 0.01	18.22 \pm 0.01	18.04 \pm 0.01	17.92 \pm 0.01
1.47	6.6	19.70 \pm 0.01	19.51 \pm 0.01	19.41 \pm 0.02	19.28 \pm 0.02	19.11 \pm 0.02	18.96 \pm 0.03
2.39	15.0	20.26 \pm 0.03	19.99 \pm 0.01	19.91 \pm 0.01	19.79 \pm 0.02	19.62 \pm 0.02	19.45 \pm 0.02
3.41	13.8	20.58 \pm 0.01	20.38 \pm 0.01	20.28 \pm 0.02	20.15 \pm 0.03	19.95 \pm 0.03	19.80 \pm 0.04
4.39	16.8	20.87 \pm 0.01	20.66 \pm 0.01	20.56 \pm 0.02	20.44 \pm 0.03	20.32 \pm 0.04	20.00 \pm 0.04
5.38	8.4	21.11 \pm 0.02	20.89 \pm 0.02	20.81 \pm 0.04	20.59 \pm 0.04	20.39 \pm 0.05	20.12 \pm 0.06
6.39	8.4	21.27 \pm 0.02	21.06 \pm 0.02	20.95 \pm 0.05	20.72 \pm 0.06	20.50 \pm 0.07	20.35 \pm 0.09
7.38	9.0	21.38 \pm 0.02	21.17 \pm 0.02	21.08 \pm 0.04	20.96 \pm 0.05	20.73 \pm 0.06	20.50 \pm 0.07
8.37	8.4	21.52 \pm 0.04	21.39 \pm 0.04	21.43 \pm 0.11	20.95 \pm 0.08	20.75 \pm 0.12	20.41 \pm 0.11
9.37	8.4	21.54 \pm 0.02	21.37 \pm 0.02	21.22 \pm 0.05	21.10 \pm 0.06	20.89 \pm 0.08	20.55 \pm 0.08
10.36	6.0	21.61 \pm 0.03	21.47 \pm 0.03	21.42 \pm 0.07	21.23 \pm 0.09	20.83 \pm 0.09	20.64 \pm 0.11
11.35	8.4	21.71 \pm 0.02	21.50 \pm 0.02	21.31 \pm 0.05	21.15 \pm 0.07	20.92 \pm 0.08	20.91 \pm 0.12
12.35	7.8	21.78 \pm 0.03	21.57 \pm 0.03	21.48 \pm 0.07	21.35 \pm 0.10	21.38 \pm 0.16	20.91 \pm 0.15
13.36	8.4	21.93 \pm 0.03	21.69 \pm 0.02	21.60 \pm 0.06	21.49 \pm 0.08	21.16 \pm 0.08	21.02 \pm 0.10
14.41	14.4	22.01 \pm 0.03	21.83 \pm 0.02	21.81 \pm 0.07	21.63 \pm 0.08	21.40 \pm 0.11	21.10 \pm 0.12
15.36	8.4	22.24 \pm 0.05	22.00 \pm 0.04	21.76 \pm 0.09	21.92 \pm 0.14	21.85 \pm 0.18	21.11 \pm 0.14
16.34	8.4	22.33 \pm 0.05	22.12 \pm 0.04	21.83 \pm 0.09	21.78 \pm 0.14	21.39 \pm 0.14	21.33 \pm 0.19
19.32	8.4	22.58 \pm 0.07	22.34 \pm 0.07	22.18 \pm 0.15	22.51 \pm 0.36	21.50 \pm 0.22	21.04 \pm 0.23
20.32	7.8	22.82 \pm 0.11	22.51 \pm 0.09	22.41 \pm 0.18	22.14 \pm 0.18	22.03 \pm 0.23	21.77 \pm 0.24
21.39	16.8	22.61 \pm 0.13	22.54 \pm 0.14	> 22.54	> 22.23	> 21.80	21.05 \pm 0.28
22.32	8.4	22.81 \pm 0.12	22.56 \pm 0.11	22.61 \pm 0.22	22.39 \pm 0.24	22.34 \pm 0.31	22.05 \pm 0.34
23.38	15.6	22.84 \pm 0.11	22.91 \pm 0.13	22.48 \pm 0.11	-	21.87 \pm 0.10	-
24.38	16.2	22.90 \pm 0.16	22.87 \pm 0.17	23.14 \pm 0.27	-	21.98 \pm 0.12	-
25.39	18.0	22.85 \pm 0.13	22.70 \pm 0.13	22.66 \pm 0.15	-	22.43 \pm 0.18	-
26.37	16.2	23.03 \pm 0.11	22.91 \pm 0.11	22.86 \pm 0.15	-	22.43 \pm 0.17	-
39.39	8.4	24.10 \pm 0.23	23.75 \pm 0.19	-	-	-	-
40.39	7.2	23.71 \pm 0.17	23.75 \pm 0.20	-	-	-	-
41.39	7.2	23.98 \pm 0.22	23.60 \pm 0.17	-	-	-	-
41.89	5.4	-	-	23.57 \pm 0.32	> 23.32	> 22.89	> 22.49
43.31	12.0	> 24.33	23.64 \pm 0.21	-	-	-	-
44.36	70.8	24.01 \pm 0.22	23.72 \pm 0.18	-	-	-	-
52.92	190.2	> 23.54	-	-	-	-	-
53.92	307.8	-	24.08 \pm 0.27	23.86 \pm 0.33	-	> 23.36	-

Magnitudes are in AB system and are not corrected for galactic extinction.